Nanoscale Advances

ROYAL SOCIETY OF CHEMISTRY

PAPER

View Article Online
View Journal | View Issue



Cite this: *Nanoscale Adv.*, 2020, **2**, 5271

# Prediction of two-dimensional $CP_3$ as a promising electrode material with a record-high capacity for Na ions†

Zishuang Cheng, [a] Xiaoming Zhang, *[ab] Hui Zhang,[a] Jianbo Gao,[c] Heyan Liu,[ab] Xiao Yu,[ab] Xuefang Dai,[a] Guodong Liu [a] and Guifeng Chen*[a]

Borophene with a maximum Li/Na capacity of 1984 mA h $g^{-1}$ (nanoscale 2016, 8, 15 340–15 347) has shown the highest capacity among two-dimensional (2-D) anode materials identified so far. Herein, we report the record break for Na-ion using a newly proposed 2-D material, namely, $CP_3$. We fully investigated Li- and Na-ion adsorption and diffusion processes on a $CP_3$ monolayer. We found that the material can enable stable Li/Na adsorption considering charge accumulation on $CP_3$ surfaces. The ion diffusion barriers for Li and Na were identified to be 98 meV and 356 meV, respectively. These values were comparable or smaller than those of the typical high-capacity electrode materials such as borophene. Most remarkably, the maximum Na capacity in $CP_3$ monolayer can reach up to 2298.9 mA h $g^{-1}$, which breaks the value recorded using borophene (1984 mA h $g^{-1}$). Our work highly promises that the 2-D $CP_3$ material could serve as an outstanding electrode material for Na-ion batteries with an extremely high storage capacity.

Received 5th September 2020
Accepted 23rd September 2020

DOI: 10.1039/d0na00746c

rsc.li/nanoscale-advances



## 1. Introduction

Li-ion battery (LIB) technology has been one of the most successful breakthroughs in recent decades. LIBs are currently used in various fields because of their high performances on energy storage and electrical operation.[1–5] Meanwhile, they are still suffering from bottlenecks for application in large-scale electrical devices because of intrinsic issues such as safety and costs.[6–10] To relieve these issues, continuous efforts have been made on two aspects. One aspect focuses on developing high-performance and cost-effective LIB electrode materials. For this consideration, two-dimensional (2-D) electrodes fall into the spotlight, because their unique geometric configurations can favor the ion diffusion and storage processes.[11–19] As accompanied, it has seen an explosion of 2-D electrode development in recent years, nearly covering all layered materials.[20–40] For the other aspect, great efforts were made on developing other types of ion batteries.[41–47] Among various potential ion batteries, Na-ion batteries (NIBs) have attracted much attention because of excellent security, low costs, and similar operating mechanisms with LIBs.[21–23,32] There has already been a rapid progress in NIB development; however, further development of LIBs face crucial challenges. One of the challenges is the lack of excellent LIB anode material, in particular those that can enable high capacity. Currently, the storage capacity of 2-D anode materials for NIBs is mostly in the range of 500–800 mA h $g^{-1}$; hence, there is an urgently need to explore excellent LIB anode materials that can enable higher capacities.

In 1970s, two typical layered materials, namely, $GeP_3$ and $SnP_3$, have been synthesized.[48–50] Soon after, the great feasibility of exfoliating $GeP_3$ and $SnP_3$ monolayers from their bulk materials has been theoretically reported.[51–54] Besides, it was found that these freestanding monolayers possess good thermodynamic and mechanical stabilities, which can exist steadily. As it is known, carbon, germanium and tin (C, Ge and Sn) belong to the same group in the periodic table of elements. Then, one may wonder whether the material of $CP_3$ can stably exist? Whether it is a layered material like $GeP_3$ and $SnP_3$? Further, is it possible to peel off monolayer from the bulk? These questions have been solved by the following studies. Ramzan *et al.* reported for the first time the excellent dynamic stability of $CP_3$ layered materials, which have a similar structure to $GeP_3$ and $SnP_3$ counterparts.[55] Immediately after, Sarkar *et al.* reported that the monolayer form of $CP_3$ has a relatively low cleavage energy, which can be readily cleaved from its bulk phases like other layered materials.[56]

In this work, we report for the first time that 2-D $CP_3$ is a very promising electrode material for LIBs and NIBs. As realized by

[a]School of Materials Science and Engineering, Hebei University of Technology, Tianjin 300130, China. E-mail: zhangxiaoming87@hebut.edu.cn; cgfchen@hebut.edu.cn
[b]State Key Laboratory of Baiyunobo Rare Earth Resource Researches and Comprehensive Utilization, Baotou Research Institute of Rare Earths, Baotou 014030, China
[c]Centre of Excellence for Advanced Materials, Dongguan 523808, China

† Electronic supplementary information (ESI) available. See DOI: 10.1039/d0na00746c

first-principles calculations, we have thoroughly simulated the Li/Na atom adsorption and diffusion processes on $CP_3$ monolayers. We realize that the $CP_3$ monolayer can enable stable Li/Na adsorption and considerable charge transfers are observed during the period. The $CP_3$ electrode hosts good conductivity, considering the definite metallic electronic structures both before and after adsorptions. The ion diffusion path and the minimum migration barriers for Li/Na atoms on $CP_3$ monolayer are obtained, which are comparable or lower than those of 2-D electrodes with high storage capacity. Besides, the storage capacity and the average open circuit voltage have been systematically investigated. The results indicated that the $CP_3$ monolayer has a low average open circuit voltage for Li/Na, which is suitable to be used as an anode material. Most excitingly, the maximum capacity of the $CP_3$ monolayer for Na-ion has reached a new record for 2-D anode materials, which is 2298.9 mA h $g^{-1}$. In particular, 2-D $CP_3$ can provide higher capacity (2298.9 mA h $g^{-1}$ *versus* 1984 mA h $g^{-1}$) than the famous anode material borophene[23] with a comparable diffusion barrier (356 meV *versus* 340 meV).

## 2. Computational details

In this work, we performed the first-principles calculations using the Vienna *ab initio* simulation package (VASP),[57] based on density functional theory (DFT).[58] For the exchange-correlation potential, we applied the generalized gradient approximation (GGA) of the Perdew–Burke–Ernzerhof (PBE) functional.[59,60] The cutoff energy was set as 500 eV during the calculations. A vacuum space with a thickness of 30 Å was built in the bare $CP_3$ monolayer to avoid artificial interaction between two single monolayers. During the calculations, the long-range van der Waals interactions were taken into account by using the DFT-D2 method.[61] The Brillouin zone was sampled with a $7 \times 7 \times 1$ Monkhorst–Pack *k*-point mesh for the geometrical optimization and with a $9 \times 9 \times 1$ *k*-mesh for the calculations of the electronic structure and atomic adsorptions. All atomic positions were fully relaxed during the calculations, and the force and energy convergence criteria were set as 0.01 eV $Å^{-1}$ and $10^{-6}$ eV, respectively. To investigate the dynamical stability of the $CP_3$ monolayer, the phonon spectra was calculated using the PHONOPY package.[62,63] The climbing-image nudged elastic band (CI-NEB) method was used to obtain the diffusion barrier height during the ion diffusion process.[64,65]

## 3. Results and discussions

### 3.1 Structure and stability of the $CP_3$ monolayer

As shown in Fig. 1(a), the bulk phase of $CP_3$ material has the so-called ABC-type layered structure (the space group is $R\bar{3}m$), which is similar to the $GeP_3$ and $SnP_3$ counterparts. Fig. 1(b) shows the structure of the $CP_3$ monolayer. Sarkar *et al.* have proposed two potential fabrication methods of the $CP_3$ monolayer.[56] For the first one, it may be directly cleaved from its layered bulk structure, and shown by the process in Fig. 1(a) and (b). Here, we evaluated the cleavage energy for the $CP_3$ monolayer. A five-layer system was used in our calculations, and the computation details are displayed in the ESI.† The cleavage energy of the $CP_3$ monolayer was calculated to be 0.65 J $m^{-2}$, which well agrees with the previous work (0.57 J $m^{-2}$).[56] This cleavage energy was lower than the DFT-calculated exfoliation energy for $Ca_2N$ (1.08 J $m^{-2}$),[66] $InP_3$ (1.32 J $m^{-2}$),[67] and $GeP_3$ (1.14 J $m^{-2}$).[68] For this consideration, the $CP_3$ monolayer was quite promising to be exfoliated experimentally from its bulk phase. Besides, Sarkar *et al.* proposed that the $CP_3$ monolayer was promising to be synthesized by doping C atoms into blue phosphorene,[56] as displayed by the process in Fig. 1(c).

In addition, we wanted to further ensure the stability of the $CP_3$ monolayer. We estimated the cohesive energy ($E_c$) of the $CP_3$ monolayer, which can be described as follows:

$$E_c = (E_{total} - mE_C - nE_P)/(m + n) \quad (1)$$

In this equation, $E_{total}$, $E_C$, and $E_P$ are on behalf of the energies of the $CP_3$ monolayer, single C and P atoms, respectively; $n$ and $m$ are the number of C and P atoms in the $CP_3$ monolayer. The calculated formation energy is −4.12 eV per unit cell, which is consistent with previous results.[56] In addition, it suggests that the $CP_3$ monolayer is energetically stable.

We make further discussions on the structure of the $CP_3$ monolayer, and top and side views are shown in Fig. 2(a) and (b), respectively. In the structure, we can find that each C atom bonds with three P atoms, and each P atom bonds with one C atom and two P atoms. Such bonding forms the connection of the $P_6$ ring and $C_2P_4$ ring, as shown by the top view in Fig. 2(a).

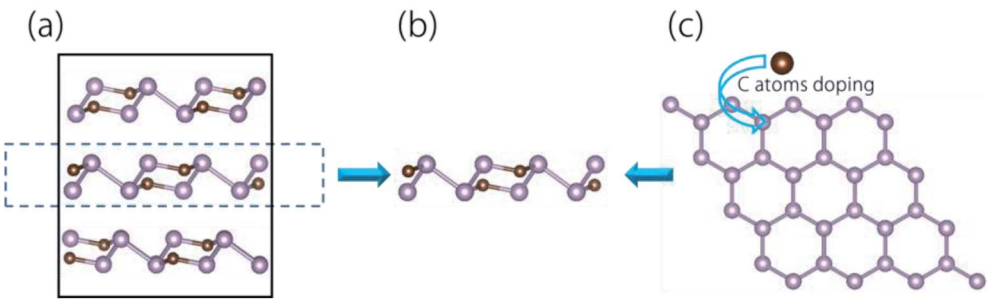


Fig. 1 (a) Optimized structure of bulk $CP_3$ with a $2 \times 2 \times 1$ supercell. (b) Crystal structure of the $CP_3$ monolayer delaminated from bulk $CP_3$. (c) C atoms doping into blue phosphorene, showing another potential $CP_3$ monolayer synthesis process.

 

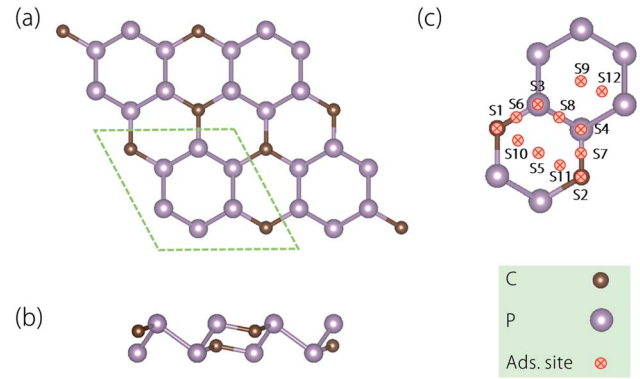


Fig. 2 Crystal structures of the $CP_3$ monolayer in (a) the top and (b) the side views. (c) The considered adsorption sites (denoted as S1–S12) on the surface of the $CP_3$ monolayer (top view).

The optimized lattice constants of the $CP_3$ monolayer is 6.22 Å, and the length of the C–P bond and P–P bond is 1.78 Å and 2.28 Å, respectively. These results are in good agreement with the previous proposal.[56] Based on the optimized structure, we study the dynamical stability of the $CP_3$ monolayer. The resulting phonon dispersion is displayed in Fig. 3(a). Apparently, one finds no imaginary frequency in the phonon spectra. Thus, the $CP_3$ monolayer is believed to be dynamically stable. In addition, we show the band structure and density of state (DOSs) of the $CP_3$ monolayer in Fig. 3(c) and (d), respectively. We can find that the $CP_3$ monolayer shows a definite metallic electronic structure. This can enable sound conductivity when applied as an electrode material. Moreover, from the DOSs in Fig. 3(d), one can find that the electronic states near the Fermi energy are mainly provided by the p orbitals of C and P atoms.

### 3.2 Ion adsorption and diffusion

Then, we investigate the ion adsorption and diffusion on the $CP_3$ monolayer. Herein, we focus on the cases for Li and Na, and the $2 \times 2$ supercell $CP_3$ monolayer is considered as the substrate for the adsorption. By lattice symmetry of the $CP_3$ monolayer, we consider nine typical adsorption sites. As shown in Fig. 2(c), these adsorption sites are denoted as S1–S12 (among them, S1–S4 are the top sites, S5 and S9 are the hollow sites, S6–S8 and S10–S12 are the bridge sites). The adsorption energy ($E_{ad}$) of Li/Na atoms on the $CP_3$ monolayer is defined as follows:

$$E_{ad} = E_{Li/Na+CP_3} - E_{CP_3} - E_{Li/Na} \quad (2)$$

where $E_{Li/Na}$ is the energy per atom for the bulk metal Li/Na, $E_{Li/Na+CP_3}$ and $E_{CP_3}$ are the total energies of the $CP_3$ monolayer after and before Li/Na adsorption. A negative value of adsorption energy means that Li/Na atoms tend to adsorb onto the $CP_3$ monolayer, instead of forming a bulk metal. The calculated adsorption energies for Li/Na are shown in Fig. 4(a). All values of adsorption energy are negative, which indicates that Li/Na atoms can stably adsorb onto the $CP_3$ monolayer.

After examining the optimized structure, we found that the Li atom at the S2, S4, and S7 sites would automatically shift to the bridge site (nearby S7, for clarity, we redefine this new adsorption site as S7); the Li atom at the S5 site would move to the S11 site; the Li atom at the S6 and S10 sites would move to the S1 one and that at the S3, S8, and S12 sites would move to the S9 one. The occasion for Na is slightly different. Adatoms at the S4, S5, S7, and S11 sites would automatically shift to the S2 site; the Na atom at the S3, S8, and S12 sites would move to the S9 one; the Na atom at the S6 and S10 sites would move to the S1 one. To sum up, Li has four stable adsorption sites on the $CP_3$

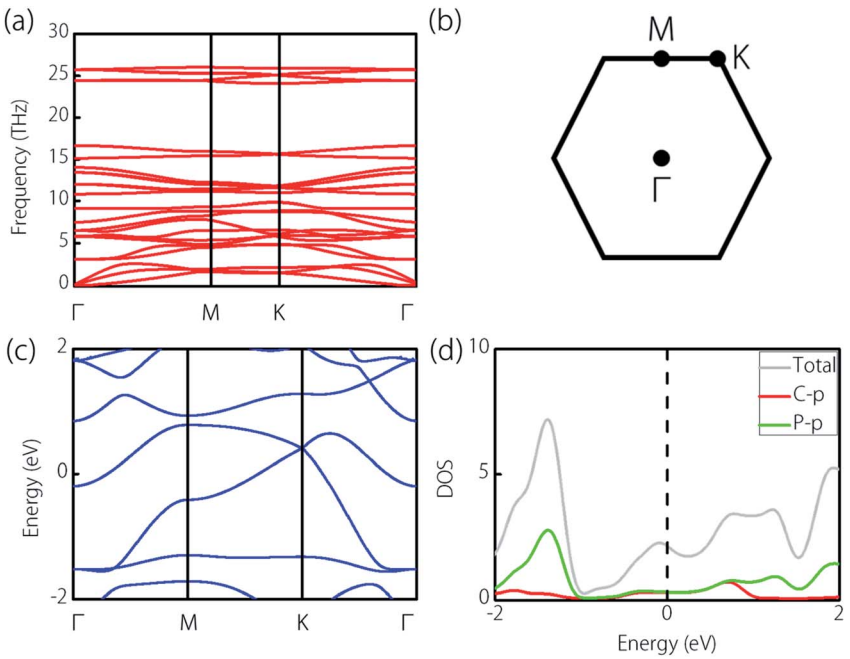


Fig. 3 (a) Phonon spectra of the fully relaxed $CP_3$ monolayer. (b) 2-D Brillouin zone of the $CP_3$ monolayer. (c) Band structures of the $CP_3$ monolayer. (d) Total and projected density of states of the $CP_3$ monolayer.

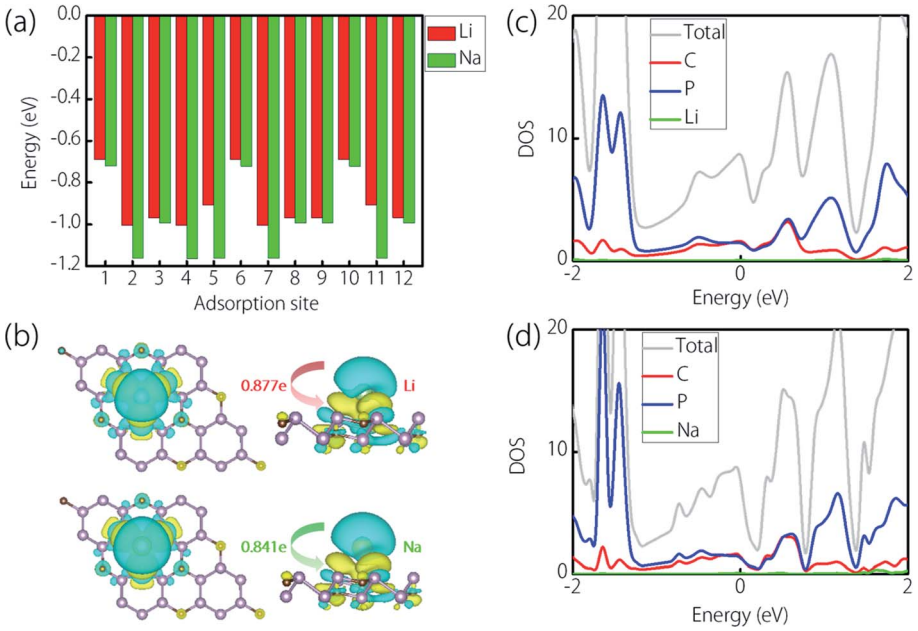


Fig. 4 (a) Li/Na adsorption energies of the twelve possible adsorption sites on the surface of the $CP_3$ monolayer. (b) Maps of charge density difference in the $CP_3$ monolayer with Li/Na adsorption as well as the amounts of charge transfer. (c) and (d) Density of states (DOS) for Li- and Na-adsorbed $CP_3$ monolayers, respectively.

monolayer, while Na has three stable adsorption sites on it. For these sites, as for Li, the stability is in the order: S7 > S9 > S11 > S1 (−1.005 eV < −0.968 eV < −0.907 eV < −0.689 eV). With regard to Na, the stability order is S2 > S9 > S1 (−1.163 eV < −0.993 eV < −0.721 eV). Besides, we compared the adsorption height at different sites, we found that the order is S11 < S7 < S9 < S1 for Li (which are 1.707 Å < 1.908 Å < 2.323 Å < 2.375 Å), and S2 < S9 < S1 for Na (which are 1.973 Å < 2.799 Å < 2.849 Å). In general, these values show a trend that the lower the ion adsorption height, the more stable the adsorption that the site can enable.

To explore the charge transfer of Li/Na atoms and the $CP_3$ monolayer, we calculated the charge density difference (CDD) during the ion adsorption. Here, the stable adsorption site (S1) was applied. As shown in Fig. 4(b), the green regions represent charge accumulation and the cyan regions represent charge depletion. We can clearly observe the obvious charge transfers to the $CP_3$ monolayer from Li/Na atoms. By the way, we also calculated the specific amount of the transferred charge using the Bader charge calculations.[69] The results indicated that the transferred charge is 0.877*e* per atom for Li and 0.841*e* per atom for Na, respectively. Therefore, we realize that Li/Na atoms are chemically adsorbed on the $CP_3$ monolayer. In addition, we displayed the projected density of states (PDOSs) for Li/Na atoms adsorbed on the $CP_3$ monolayer in Fig. 4(c) and (d), respectively. We can clearly find that the $CP_3$ monolayer still possesses metallic conductivity after the adsorption, which enables the great feasibility of the $CP_3$ monolayer as an electrode material for ion batteries.

The diffusion performance of adatoms on the electrode is closely related to its rate capability, and low diffusion is highly required for electrode materials. Here, we estimated the Li/Na diffusion ability on the $CP_3$ monolayer using the CI-NEB calculations. On account of the structural symmetry and adsorption sites, three most possible ion diffusion paths (P–A, P–B, and P–C) were taken into account for Li, and two most possible ion diffusion paths (P–A and P–B) were taken into account for Na. These are shown in Fig. 5(a). As for Li, the diffusion route for P–A is that: the Li atom moves from the S7 site to S11 one, and finally moves to another S7 one. In P–B, the Li atom moves from the S7 site to the S9 one, and finally moves to another S7 one. In P–C, the Li atom moves from the S7 site to the S1 one, and finally moves to another S7 one. As for Na, the diffusion route for P–A is that: the Na atom moves from the S2 site to S9 one, and finally moves to another S2 one. In P–B, the

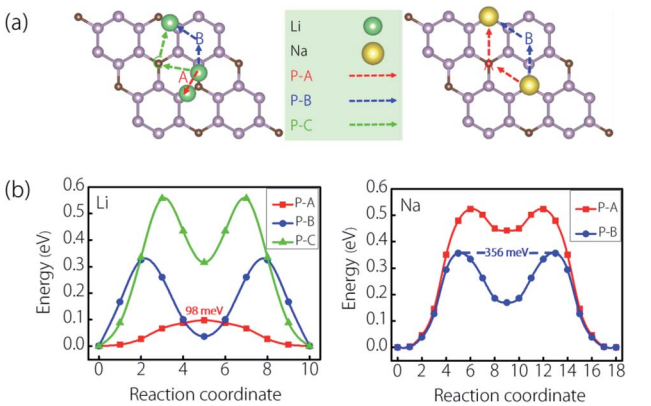


Fig. 5 (a) Potential Li/Na ion diffusion paths and (b) the corresponding ion diffusion profiles on the $CP_3$ monolayer as well as the size of the minimum diffusion barrier.

 

Na atom moves from the S2 site to the S1 one, and finally moves to another S2 one. The calculated diffusion profiles are shown in Fig. 5(b). We can find that the Li diffusion energy for P–A is lower than those of P–B and P–C, while the Na diffusion energy for P–B is the lower than that of P–A. Herein, the diffusion barrier is as low as 98 meV for Li and 356 meV for Na. These diffusion barriers are moderate when comparing with typical 2-D electrode materials. For example, they are a bit higher (or comparable) than electrode materials such as $Ti_3C_2$ (68 meV for Li and 96 meV for Na),[26] blue-phosphorene (130 meV for Li and 110 meV for Na),[70,71] and so on. However, they are much lower than graphene (370 meV for Li),[22] $MoN_2$ (780 meV for Li, and 560 meV for Na),[33] and $\beta_{12}/\chi_3$ borophene (600/660 meV for Li, and 300/340 meV for Na).[23,24] These results indicated that the $CP_3$ monolayer would enable good ion diffusion ability when applied as battery electrodes.

### 3.3 Storage capacity and open circuit voltage

Besides the diffusion barrier, the storage capacity and the average open circuit voltage are important characters for the electrode materials. To obtain the maximum possible storage of Li/Na, we calculated the average adsorption energies of Li/Na atoms for layers. Here, we still use the 2 × 2 supercell of the $CP_3$ monolayer as the substrate, then display the adatoms on the $CP_3$ monolayer layer by layer. Therefore, the average adsorption energy in each layer ($E_{ave}$) can be defined as follows:

$$E_{ave} = (E_{Li_{8n}/Na_{8n}+C_8P_{24}} - E_{Li_{(n-1)8}/Na_{(n-1)8}+C_8P_{24}} - 8E_{Li/Na})/8 \quad (3)$$

Here, $E_{Li/Na}$ is the energy per atom in bulk Li/Na metals; $E_{Li_{8n}/Na_{8n}+C_8P_{24}}$ and $E_{Li_{(n-1)8}/Na_{(n-1)8}+C_8P_{24}}$ are the total energies of the $CP_3$ monolayer with "$n$" and "$n-1$" Li/Na adsorption layers. The number "8" represents eight Li/Na atoms adsorbed on both sides of the 2 × 2 supercell per layer. According to the adsorption energies, the adsorption sequence for Li can be described as: S7 (the first layer) – S9 (the second layer) – S11 (the third layer) – S1 (the fourth layer), and the adsorption sequence for Na can be described as: S2 (the first layer) – S9 (the second layer) – S1 (the third layer).

For Li adsorption on the $CP_3$ monolayer, we found that only two layers can be stably adsorbed with negative $E_{ave}$, and the values are −0.893 eV for the first layer and −0.172 eV for the second layer, respectively. As the results, we realize that the $CP_3$ monolayer can at most enable 18 Li atoms adsorbed on the surface. The optimized structures for one and two adsorption layers are shown in Fig. 6(a). In addition, and the other side views of optimized structures are provided in the ESI.† As for Na, we are delighted to find that the $CP_3$ monolayer can enable extremely high ability for Na adsorption. With the triple-layer configuration (S2–S9–S1) as the period, we are surprised to find that three of such adsorption periods can show negative adsorption energy. In addition, the average adsorption energy is −0.600 eV for the first triple-layers, −0.120 eV for the second triple-layers, and −0.196 eV for the third triple-layers, respectively. Therefore, nine Na layers (totally 72 Na atoms) can be adsorbed on the $CP_3$ monolayer. Likewise, we show these optimized structures in Fig. 6(b), and the other side views of them

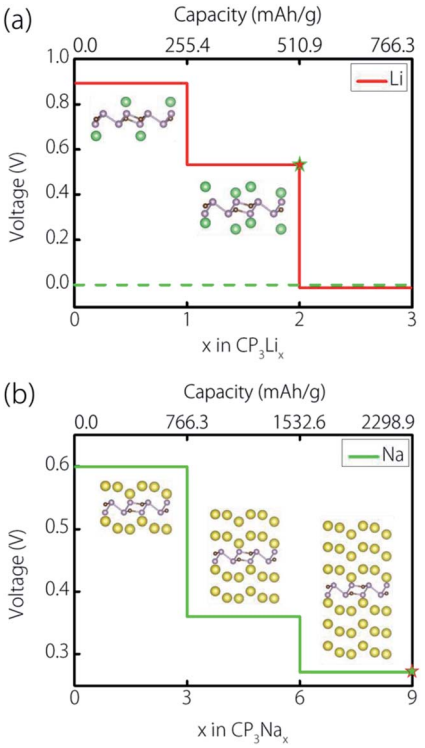


Fig. 6 Voltage profiles and specific ion storage capacities for (a) Li and (b) Na adsorption on the $CP_3$ monolayer. In (a) and (b), the optimized structures of $CP_3Li_x$ and $CP_3Na_x$ on the step and the maximum Li and Na capacities (the star) are provided.

are provided in the ESI.† In addition, we investigated the mechanical property of the $CP_3$ monolayer before and after adsorption. The elastic constants, the Young modulus and the Poisson ratio were calculated (the results are shown in the ESI†). The elastic constants for all the cases satisfy the Born criteria ($C_{44} > 0$; $C_{11}C_{22} - C_{12}^2 > 0$). This indicates that the $CP_3$ monolayer is mechanically stable before and after Li/Na adsorption.

As for $CP_3$ monolayer, the typical half–cell reaction can be defined as follows:

$$CP_3 + xLi^+/Na^+ + xe^- \leftrightarrow Li/NaCP_3 \quad (4)$$

Accordingly, we can estimate the open circuit voltage (OCV) from the following equation:

$$V_{ave} = (E_{CP_3} + xE_{Li/Na} - E_{Li/NaCP_3})/xe \quad (5)$$

where $x$ represents the number of Li/Na atoms, and other parameters are the same for those in eqn (1). The voltage profiles are provided in Fig. 6(a) and (b), respectively. In the figures, we find the OCV for Li is in the range of 0.53–0.89 V, and that for Na is in the range of 0.27–0.60 V. These OCV values suggest that the $CP_3$ monolayer is feasible to become an electrode material for LIBs and NIBs.

The above discussions show that a 2 × 2 supercell could accommodate up to 18 atoms of Li and 72 atoms of Na, respectively. Such adsorptions correspond to the chemical

stoichiometry of $CP_3Li_2$ and $CP_3Na_9$. Finally, we can obtain the maximum storage capacity ($C_m$) using the following equation:

$$C_m = x_m F / M_{CP_3}. \quad (6)$$

In this equation, $x_m$ is the maximum Li/Na concentration (for the current case, $x_m = 2$ for Li; $x_m = 9$ for Na); $F$ is the Faraday constant (26.8 A h $mol^{-1}$); and $M_{CP_3}$ is the molecular mass of $CP_3$. As a result, the storage capacities of Li and Na on the $CP_3$ monolayer are 510.9 mA h $g^{-1}$ and 2298.9 mA h $g^{-1}$, respectively.

Before ending, we want to emphasize the extremely high capacity for Na on the $CP_3$ monolayer. Here, in Fig. 7, we list some typical 2-D anode materials for the maximum capacity of NIBs. They include $Ti_3C_2$ (352 mA h $g^{-1}$),[26] $Mn_2C$ (444 mA h $g^{-1}$),[72] 2-D GaN (625 mA h $g^{-1}$),[73] blue phosphorene (865 mA h $g^{-1}$),[71] black phosphorene (865 mA h $g^{-1}$),[72] $MnSb_2S_4$ (879 mA h $g^{-1}$),[74] $GeP_3$ (1295 mA h $g^{-1}$),[75] and $\beta_{12}/\chi_3$ borophene (1240/1984 mA h $g^{-1}$).[23,24] It is very exciting to note that the maximum Na-ion capacity of the current $CP_3$ monolayer is up to 2298.9 mA h $g^{-1}$, which is much higher than all the examples listed in Fig. 7. We also examined the capacities of other 2-D Na anodes reported in the literature, and to the best of our knowledge, we found that the $CP_3$ monolayer still has the highest Na-ion storage capacity. As we all know, high storage capacity is one of the most crucial performances for electrode materials. The results in our work indicate that the $CP_3$ monolayer can be expected to be a 2-D anode material for NIBs with the record-high storage capacity.

### 3.4 Additional discussions

Before ending, we have several remarks. First, we have recently become aware of a similar work that focused on the $CP_3$ monolayer.[78] For the first time, the literature proposed the feasibility of the $CP_3$ monolayer as a potential electrode material for Na-ion batteries.[78] Although the literature has focused on the same material, we want to point out that our work still has two crucial differences. First, besides the Na-ion batteries, we studied the feasibility of the $CP_3$ monolayer as an electrode for Li-ion batteries and found that the material shows an extremely low diffusion barrier of 98 meV and a moderate storage capacity of 510.9 mA h $g^{-1}$ for Li ions, while the literature did not discuss the case of Li. Second and most importantly, the literature has greatly underestimated the capacity for Na (1022 mA h $g^{-1}$).

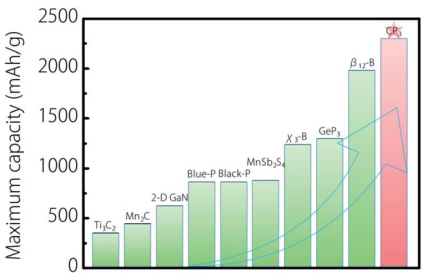


Fig. 7 Comparison of $CP_3$ monolayer with typical 2-D anode materials for the maximum Na-ion capacity.

This may imply that some adsorption possibilities were not taken into account. In our work, we found that a $CP_3$ substrate can support more Na adsorption than those reported in the literature. We have comprehensively considered twelve possible adsorption sites and found three favorable adsorption sites after full geometrical relaxations. Our calculations identified one more stable adsorption site than reported in the literature, which locates on the top of one C atom [S1 site in Fig. 2(c)]. In our calculations, at the beginning, we add Na atoms layer by layer on the $CP_3$ substrate. Very interestingly, after adding three layers of Na atoms, we found that the $CP_3$ substrate can stably adsorb more Na atoms. To simplify, we consider three layers of Na atoms as a period. Our calculations showed that the $CP_3$ substrate can adsorb up to three periods of such adsorption. As the result, the maximum capacity for Na is in fact 2298.9 mA h $g^{-1}$. This capacity is the highest among known 2-D anode materials for Na ions. The record-high capacity is the most important innovation point in this work.

Second, our calculations show that the $CP_3$ monolayer can support the multilayer adsorption for Na ions, while not for Li ions. For the case of Li, the $CP_3$ monolayer can stably adsorb two layers. When the third layer is displayed, we can find that the final structure breaks down [see ESI†]. The potential reason is that the adsorption height for Li is much lower than that for Na (1.795 Å *vs.* 2.104 Å for the first layer; 2.516 Å *vs.* 3.175 Å for the second layer). This induces more powerful interaction between the Li adatoms and $CP_3$ monolayer than that of Na; hence, the structure collapses when multiple layers of Li are displayed. In addition, we found that such phenomenon also happens in many other 2-D electrode materials. For instance: $Ca_2N$ and $Sr_2N$ can adsorb multiple layers of Na but no Li;[32] $GeP_3$,[75,76] $MoN_2$,[33] and GeS[68] can adsorb multiple layers of Na but only one layer of Li.

Third, we want to point out that the supercell size of the substrate sometimes would affect the adsorption and ion diffusion properties. In the above discussions, the 2 × 2 supercell of the $CP_3$ monolayer was applied. We tested the Li/Na adsorption and diffusion processes in the 3 × 3 and the 4 × 4 supercells. We found that the most favorable adsorption site and the maximum capacity are not changed in the 3 × 3 and the 4 × 4 supercells. In addition, the minimum diffusion barrier is only slightly changed for Na (356 meV for 2 × 2 supercell *vs.* 336 meV for 3 × 3 supercell *vs.* 329 meV for 4 × 4 supercell). These results indicated that the 2 × 2 supercell of the $CP_3$ monolayer was suitable for investigating the adsorption and diffusion processes in this work. Moreover, the size of the 2 × 2 supercell was also applied to similar structures such as $GeP_3$ (ref. 75 and 76) and $SnP_3$.[77]

## 4. Conclusion

In conclusion, we have systematically investigated the performance of a $CP_3$ monolayer as a potential LIB/NIB anode material by the first-principles calculations. We realized that Li/Na atoms could steadily adsorb onto the $CP_3$ monolayer surface, and the corresponding adsorption energies and adsorption sites were obtained. We showed that the $CP_3$ monolayer

 

possesses good metallic conductivity before and after adsorptions, which is desirable for electrode materials. In addition, the average OCV and ion diffusion paths have been determined. The results indicated that the lowest diffusion barrier is 98 meV for Li and 356 meV for Na, which are comparable or much lower than those of most high-capacity 2-D electrode materials such as borophene. Most attractively, we realized that the storage capacity of Na on the $CP_3$ monolayer can be up to 2298.9 mA h $g^{-1}$, which is the highest among 2-D NIB anodes identified so far. To sum up, these outstanding performances suggest that the $CP_3$ monolayer is a potential NIB anode material with extremely high storage capacity.

## Conflicts of interest

There are no conflicts to declare.

## Acknowledgements

This work was supported by National Natural Science Foundation of China (grant numbers 51871089, 61674051), the Program for Guangdong Introducing Innovative and Enterpreneurial Teams (No. 2016ZT06G025), and the open subject of State Key Laboratory of Research and Comprehensive Utilization of Rare Earth Resources in Baiyun Ebo (No. 2020z2123). One of the authors (X. M. Zhang) acknowledges the financial support from Young Elite Scientists Sponsorship Program by Tianjin.

## References

1 S. Liu, W. Xu, C. Ding, J. Yu, D. Fang, Y. Ding and H. Hou, Boosting electrochemical performance of electrospun silicon-based anode materials for lithium-ion battery by surface coating a second layer of carbon, *Appl. Surf. Sci.*, 2019, **494**, 94–100.

2 H. D. Chen, K. X. Shen, X. H. Hou, G. Z. Zhang, S. F. Wang, F. M. Chen, L. J. Fu, H. Q. Qin, Y. C. Xia and G. F. Zhou, Si-based anode with hierarchical protective function and hollow ring-like carbon matrix for high performance lithium ion batteries, *Appl. Surf. Sci.*, 2019, **470**, 496–506.

3 Q. F. Fu, R. J. Li, X. Z. Zhu, G. S. Liang, L. J. Luo, Y. J. Chen, C. F. Lin and X. S. Zhao, Design, synthesis and lithium-ion storage capability of $Al_{0.5}Nb_{24.5}O_{62}$, *J. Mater. Chem. A*, 2019, **7**, 19862–19871.

4 X. Z. Zhu, J. Xu, Y. P. Luo, Q. F. Fu, G. S. Liang, L. J. Luo, Y. J. Chen, C. F. Lin and X. S. Zhao, $MoNb_{12}O_{33}$ as a new anode material for high-capacity, safe, rapid and durable $Li^+$ storage: structural characteristics, electrochemical properties and working mechanisms, *J. Mater. Chem. A*, 2019, **7**, 6522–6532.

5 X. M. Lou, R. J. Li, X. Z. Zhu, L. J. Luo, Y. J. Chen, C. F. Lin, H. L. Li and X. S. Zhao, New anode material for lithium-ion batteries: aluminum niobate ($AlNb_{11}O_{29}$), *ACS Appl. Mater. Interfaces*, 2019, **11**, 6089–6096.

6 J. R. Dahn, T. Zheng, Y. Liu and J. S. Xue, Mechanisms for Lithium Insertion in Carbonaceous Materials, *Science*, 1995, **270**, 590–593.

7 M. Winter, J. O. Besenhard, M. E. Spahr and P. Novak, Insertion Electrode Materials for Rechargeable Lithium Batteries, *Adv. Mater.*, 1998, **10**, 725–763.

8 J. M. Tarascon, Is lithium the new gold?, *Nat. Chem.*, 2010, **2**, 510.

9 J. B. Goodenough and K. S. Park, The Li-ion rechargeable battery: a perspective, *J. Am. Chem. Soc.*, 2013, **135**, 1167–1176.

10 J. M. Tarascon and M. Armand, Issues and challenges facing rechargeable lithium batteries, *Nature*, 2001, **414**, 359–367.

11 J. Liu and X. W. Liu, Two-dimensional nanoarchitectures for lithium storage, *Adv. Mater.*, 2012, **24**, 4097–4111.

12 H. Zhang, Ultrathin two-dimensional nanomaterials, *ACS Nano*, 2015, **9**, 9451–9469.

13 C. Tan, X. Cao, X. J. Wu, Q. He, J. Yang, X. Zhang, J. Chen, W. Zhao, S. Han, G. H. Nam, M. Sindoro and H. Zhang, Recent advances in ultrathin two-dimensional nanomaterials, *Chem. Rev.*, 2017, **117**, 6225–6331.

14 N. Oyama, T. Tatsuma, T. Sato and T. Sotomura, Dimercaptan–Polyaniline Composite Electrodes for Lithium Batteries with High Energy Density, *Nature*, 1995, **373**, 598–600.

15 J. M. Tarascon and M. Armand, Issues and Challenges Facing Rechargeable Lithium Batteries, *Nature*, 2001, **414**, 359–367.

16 H. Chen, T. N. Cong, W. Yang, C. Tan, Y. Li and Y. Ding, Progress in Electrical Energy Storage System: A Critical Review, *Prog. Nat. Sci.*, 2009, **19**, 291–312.

17 B. Dunn, H. Kamath and J. M. Tarascon, Electrical Energy Storage for the Grid: A Battery of Choices, *Science*, 2011, **334**, 928–935.

18 W. Li, Y. Yang, G. Zhang and Y. W. Zhang, Ultrafast and Directional Diffusion of Lithium in Phosphorene for High-Performance Lithium-Ion Battery, *Nano Lett.*, 2015, **15**, 1691–1697.

19 D. P. Dubal, O. Ayyad, V. Ruiz and P. Gomez-Romero, Hybrid Energy Storage: the Merging of Battery and Supercapacitor Chemistries, *Chem. Soc. Rev.*, 2015, **44**, 1777–1790.

20 K. J. Naresh, B. A. Rafael, S. Vivekanand and A. Rajeev, Borophane as a Benchmate of Graphene: A Potential 2D Material for Anode of Li and Na-Ion Batteries, *ACS Appl. Mater. Interfaces*, 2017, **9**, 16148–16158.

21 J. Sun, H. W. Lee, M. Pasta, H. Yuan, G. Zheng, Y. Sun, Y. Li and Y. Cui, A Phosphorene-Graphene Hybrid Material as a High-Capacity Anode for Sodium-Ion Batteries, *Nat. Nanotechnol.*, 2015, **10**, 980–985.

22 E. Pollak, B. Geng, K. J. Jeon, I. T. Lucas, T. J. Richardson, F. Wang and R. Kostecki, The Interaction of $Li^+$ with Single-Layer and Few-Layer Graphene, *Nano Lett.*, 2010, **10**, 3386–3388.

23 X. M. Zhang, J. P. Hu, Y. H. Cheng, H. Y. Yang, Y. G. Yao and S. A. Yang, Borophene as an Extremely High Capacity Electrode Material for Li-Ion and Na-Ion Batteries, *Nanoscale*, 2016, **8**, 15340–15347.

24 H. R. Jiang, Z. Lu, M. C. Wu, F. Ciucci and T. S. Z. Borophene, A Promising Anode Material Offering High Specific Capacity and High Rate Capability for Lithium-Ion Batteries, *Nano Energy*, 2016, **23**, 97–104.

25 D. Datta, J. Li and V. B. Shenoy, Defective graphene as a high-capacity anode material for Na- and Ca-ion batteries, *ACS Appl. Mater. Interfaces*, 2014, **6**, 1788–1795.

26 D. Q. Er, J. W. Li, M. Naguib, Y. Gogotsi, V. B. ShenoyEr, D. Li, J. Naguib, M. Gogotsi and Y. Shenoy, $Ti_3C_2$ MXene as a high capacity electrode material for metal (Li, Na, K, Ca) ion batteries, *ACS Appl. Mater. Interfaces*, 2014, **6**, 11173–11179.

27 Q. Sun, Y. Dai, Y. Ma, T. Jing, W. Wei and B. Huang, *Ab initio* prediction and characterization of $Mo_2C$ monolayer as anodes for lithium-ion and sodium-ion batteries, *J. Phys. Chem. Lett.*, 2016, **7**, 937–943.

28 D. Çakır, C. Sevik, O. Gülserenc and F. M. Peetersa, $Mo_2C$ as a high capacity anode material: a first-principles study, *J. Mater. Chem. A*, 2016, **4**, 6029–6034.

29 J. Hu, B. Xu, C. Ouyang, S. A. Yang and Y. Yao, Investigations on $V_2C$ and $V_2CX_2$ (X = F, OH) Monolayer as a Promising Anode Material for Li Ion Batteries from First-Principles Calculations, *J. Phys. Chem. C*, 2014, **118**, 24274–24281.

30 J. Hu, B. Xu, C. Ouyang, Y. Zhang and S. A. Yang, Investigations on $Nb_2C$ Monolayer as Promising Anode Material for Li or Non-Li Ion Batteries from First-Principles Calculations, *RSC Adv.*, 2016, **6**, 27467–27474.

31 Q. Wan, S. Li and J. B. Liu, First-Principle Study of Li-Ion Storage of Functionalized $Ti_2C$ Monolayer with Vacancies, *ACS Appl. Mater. Interfaces*, 2018, **10**, 6369–6377.

32 J. Hu, B. Xu, S. A. Yang, S. Guan, C. Ouyang and Y. Yao, 2D Electrides as Promising Anode Materials for Na-Ion Batteries from First-Principles Study, *ACS Appl. Mater. Interfaces*, 2015, **7**, 24016–24022.

33 X. M. Zhang, Z. M. Yu, S. S. Wang, S. Guan, H. Y. Yang, Y. G. Yao and S. A. Yang, Theoretical Prediction of $MoN_2$ Monolayer as a High Capacity Electrode Material for Metal Ion Batteries, *J. Mater. Chem. A*, 2016, **4**, 15224–15231.

34 S. U. Rehman, S. A. Khan, W. Uddin, Q. U. Khan, M. Kiain, I. Mehmood, M. Sohail, M. Saeed, S. Kumar and L. Zhu, First principle study of new $W_2N$ monolayer: a promising candidate for $Li^+$ ion batteries, *Int. J. Electrochem.*, 2019, **14**, 3070–3080.

35 Z. Xu, X. Lv, J. Chen, *et al.*, DFT investigation of capacious, ultrafast and highly conductive hexagonal $Cr_2C$ and $V_2C$ monolayers as anode materials for high-performance lithium-ion batteries, *Phys. Chem. Chem. Phys.*, 2017, **19**, 7807–7819.

36 Y. Jing, Z. Zhou, C. Cabrera and Z. Chen, Metallic $VS_2$ Monolayer: A Promising 2D Anode Material for Lithium Ion Batteries, *J. Phys. Chem. C*, 2013, **117**, 25409–25413.

37 R. Bhandavat, L. David and G. Singh, Synthesis of Surface-Functionalized $WS_2$ Nanosheets and Performance as Li-Ion Battery Anodes, *J. Phys. Chem. Lett.*, 2012, **3**, 1523–1530.

38 P. He, M. Yan, G. Zhang, R. Sun, L. Chen and Q. An, Layered $VS_2$ Nanosheet-Based Aqueous Zn Ion Battery Cathode, *Adv. Energy Mater.*, 2017, **7**, 1601920.

39 S. Deng, L. Wang, T. Hou and Y. Li, Two-Dimensional $MnO_2$ as a Better Cathode Material for Lithium Ion Batteries, *J. Phys. Chem. C*, 2015, **119**, 28783–28788.

40 M. O. Guler, O. Cevher, T. Cetinkaya, *et al.*, High capacity $TiO_2$ anode materials for Li-ion batteries, *Energy Convers. Manage.*, 2013, 111–116.

41 A. Eftekhari, Potassium secondary cell based on prussian blue cathode, *J. Power Sources*, 2004, **126**, 221–228.

42 T. Ichitsubo, T. Adachi, S. Yagi and T. Doi, Potential positive electrodes for high-voltage magnesium-ion batteries, *J. Mater. Chem.*, 2011, **21**, 11764–11772.

43 C. D. Wessells, S. V. Peddada, R. A. Huggins and Y. Cui, Nickel hexacyanoferrate nanoparticle electrodes for aqueous sodium and potassium ion batteries, *Nano Lett.*, 2011, **11**, 5421–5425.

44 S. Liu, J. J. Hu, N. F. Yan, G. L. Pan, G. R. Li and X. P. Gao, Aluminum storage behavior of anatase $TiO_2$ nanotube arrays in aqueous solution for aluminum ion batteries, *Energy Environ. Sci.*, 2012, **5**, 9743–9746.

45 M. D. Slater, D. Kim, E. Lee and C. S. Johnson, Sodium-ion batteries, *Adv. Funct. Mater.*, 2013, **23**, 947–958.

46 N. Singh, T. S. Arthur, C. Ling, M. Matsui and F. Mizuno, A high energy-density tin anode for rechargeable magnesium-ion batteries, *Chem. Commun.*, 2013, **49**, 149–151.

47 D. Datta, J. Li and V. B. Shenoy, Defective graphene as a high-capacity anode material for Na- and Ca-ion batteries, *ACS Appl. Mater. Interfaces*, 2014, **6**, 1788–1795.

48 J. Gullman and O. Olofsson, The crystal structure of $SnP_3$ and a note on the crystal structure of $GeP_3$, *J. Solid State Chem.*, 1972, **5**, 441–445.

49 L. Haggstrom, J. Gullman, T. Ericsson, *et al.*, Mössbauer study of tin phosphides, *J. Solid State Chem.*, 1975, **13**, 204–207.

50 P. C. Donohue and H. S. Young, Synthesis, structure, and superconductivity of new high pressure phases in the systems GeP and GeAs, *J. Solid State Chem.*, 1970, **1**, 143–149.

51 S. Sun, F. Meng, H. Wang and Y. Ni, Novel two-dimensional semiconductor $SnP_3$: high stability, tunable bandgaps and high carrier mobility explored using first-principles calculations, *J. Mater. Chem. A*, 2018, **6**, 11890–11897.

52 Y. Jing, Y. Ma, Y. Li and T. Heine, $GeP_3$: A Small Indirect Band Gap 2D Crystal with High Carrier Mobility and Strong Interlayer Quantum Confinement, *Nano Lett.*, 2017, **17**, 1833–1838.

53 L. Feng, A. Li, P. Wang and Z. T. Liu, Novel Two-Dimensional Semiconductor $SnP_3$ with High Carrier Mobility, Good Light Absorption, and Strong Interlayer Quantum Confinement, *J. Phys. Chem. C*, 2018, **122**, 24359–24367.

54 B. Ghosh, S. Puri, A. Agarwal and S. Bhowmick, $SnP_3$: A Previously Unexplored Two-Dimensional Material, *J. Phys. Chem. C*, 2018, **122**, 18185–18191.

55 M. S. Ramzan, V. Bacic, Y. Jing and A. Kuc, Electronic Properties of a New Family of Layered Materials from Groups 14 and 15: First-Principles Simulations, *J. Phys. Chem. C*, 2019, **123**, 25470–25476.

 

56 M. Kar, R. Sarkar, S. Pal and P. Sarkar, Two-dimensional $CP_3$ monolayer and its fluorinated derivative with promising electronic and optical properties: A theoretical study, *Phys. Rev. B*, 2020, **101**, 195305.

57 G. Kresse and J. Furthmuller, Efficient Iterative Schemes for *Ab Initio* Total-Energy Calculations Using a Plane-Wave Basis Set, *Phys. Rev. B: Condens. Matter Mater. Phys.*, 1996, **54**, 11169.

58 G. Kresse and D. Joubert, From Ultrasoft Pseudopotentials to the Projector Augmented-Wave Method, *Phys. Rev. B: Condens. Matter Mater. Phys.*, 1999, **59**, 1758–1775.

59 J. P. Perdew, K. Burke and Y. Wang, Generalized Gradient Approximation for the Exchange-Correlation Hole of a Many-Electron System, *Phys. Rev. B: Condens. Matter Mater. Phys.*, 1996, **54**, 16533–16539.

60 J. P. Perdew, K. Burke and M. Ernzerhof, Generalized Gradient Approximation Made Simple, *Phys. Rev. Lett.*, 1996, **77**, 3865–3868.

61 S. Grimme, Semiempirical GGA-Type Density Functional Constructed with a Long-Range Dispersion Correction, *J. Comput. Chem.*, 2006, **27**, 1787–1799.

62 A. Togo, F. Oba and I. Tanaka, First-principles calculations of the ferroelastic transition between rutile-type and $CaCl_2$-type $SiO_2$ at high pressures, *Phys. Rev. B: Condens. Matter Mater. Phys.*, 2008, **78**, 134106.

63 X. Gonze and C. Y. Lee, Dynamical matrices, Born effective charges, dielectric permittivity tensors, and interatomic force constants from density-functional perturbation theory, *Phys. Rev. B: Condens. Matter Mater. Phys.*, 1997, **55**, 10355–10368.

64 G. Henkelman, B. P. Uberuaga and H. Jónsson, A Climbing Image Nudged Elastic Band Method for Finding Saddle Points and Minimum Energy Paths, *J. Chem. Phys.*, 2000, **113**, 9901.

65 G. Henkelman and H. Jónsson, Improved Tangent Estimate in the Nudged Elastic Band Method for Finding Minimum Energy Paths and Saddle Points, *J. Chem. Phys.*, 2000, **113**, 9978.

66 S. Zhao, Z. Li, J. Yang, *et al.*, Obtaining Two-Dimensional Electron Gas in Free Space without Resorting to Electron Doping: An Electride Based Design, *J. Am. Chem. Soc.*, 2014, **136**(38), 13313–13318.

67 N. Miao, B. Xu, N. C. Bristowe, J. Zhou and Z. Sun, Tunable Magnetism and Extraordinary Sunlight Absorbance in Indium Triphosphide Monolayer, *J. Am. Chem. Soc.*, 2017, **139**(32), 11125–11131.

68 F. Li, X. Liu, Y. Wang and Y. Li, Germanium monosulfide monolayer: a novel two-dimensional semiconductor with a high carrier mobility, *J. Mater. Chem. C*, 2016, **4**(11), 2155–2159.

69 W. Tang, E. Sanville and G. Henkelman, A Grid-Based Bader Analysis Algorithm without Lattice Bias, *J. Phys.: Condens. Matter*, 2009, **21**, 084204.

70 Q. Li, C. Duan, X. Wan, *et al.*, Theoretical Prediction of Anode Materials in Li-Ion Batteries on Layered Black and Blue Phosphorus, *J. Phys. Chem. C*, 2015, **119**, 8662–8670.

71 S. Mukherjee, L. Kavalsky and C. V. Singh, Ultrahigh storage and fast diffusion of Na and K in blue phosphorene anodes, *ACS Appl. Mater. Interfaces*, 2018, **10**, 8630–8639.

72 X. M. Zhang, W. Z. Meng, T. L. He, *et al.*, $Mn_2C$ monolayer: a superior anode material offering good conductivity, high storage capacity and ultrafast ion diffusion for Li-ion and Na-ion batteries, *Appl. Surf. Sci.*, 2020, **503**, 144091.

73 X. M. Zhang, L. Jin, X. F. Dai, G. F. Chen and G. D. Liu, Two-dimensional GaN: an excellent electrode material providing fast ion diffusion and high storage capacity for Li-ion and Na-ion batteries, *ACS Appl. Mater. Interfaces*, 2018, **10**, 38978–38984.

74 Z. Z. Zhang, Y. F. Zhang, Y. Li, J. Lin, D. Truhlar and S. P. Hua, $MnSb_2S_4$ monolayer as an anode material for metal-ion batteries, *Chem. Mater.*, 2018, **30**, 3208–3214.

75 X. Deng, X. Chen, Y. Huang, *et al.*, Two-dimensional $GeP_3$ as a high capacity anode material for non-lithium-ion batteries, *J. Phys. Chem. C*, 2019, **123**, 4721–4728.

76 C. M. Zhang, Y. L. Jiao, T. W. He, F. X. Ma, L. Z. Kou, T. Liao, S. Bottle and A. J. Du, Two-dimensional $GeP_3$ as a high capacity electrode material for Li-ion batteries, *Phys. Chem. Chem. Phys.*, 2017, **19**, 25886–25890.

77 C. S. Liu, X. L. Yang, J. Liu and X. J. Ye, Theoretical Prediction of Two-Dimensional $SnP_3$ as a Promising Anode Material for Na-Ion Batteries, *ACS Appl. Energy Mater.*, 2018, **1**, 3850–3859.

78 Z. Y. Zhao, Y. Tong, S. T. Zhang, H. Y. Xu, G. C. Yang and Y. C. Liu, Metallic $P_3C$ monolayer as anode for sodium-ion batteries, *J. Mater. Chem. A*, 2019, **7**, 405–411.